Research Article

Concept of an efficient self-startup voltage converter with dynamic maximum power point tracking for microscale thermoelectric generators

D. Merten[1] · J. A. Singer[2] · H. Fiedler[3] · S. Tappertzhofen[1]

Received: 31 January 2022 / Accepted: 10 April 2022
Published online: 25 April 2022

Abstract
Microscale Thermoelectric Generators (microTEGs) have a high application potential for energy harvesting for autonomous microsystems. In contrast to conventional thermoelectric generators, microTEGs can only supply small output-voltages. Therefore, voltage converters are required to provide supply-voltages that are sufficiently high to power microelectronics. However, for high conversion efficiency, voltage converters need to be optimized for the limited input voltage range and the typically high internal resistance of microTEGs. To overcome the limitations of conventional voltage converters we present an optimized self-startup voltage converter with dynamic maximum power point tracking. The performance potential of our concept is theoretically and experimentally analyzed. The voltage conversion interface demonstrates energy harvesting from open-circuit voltages as low as 30.7 mV, and enables independent and full start-up from 131 mV. No additional external power supply is required at any time during operation. It can be operated with a wide range of internal resistances from 20.6 to − 4 kΩ with a conversation efficiency between $\eta = 68–79\%$.

Keywords Boost converter · Dynamic maximum power point tracking · Meissner oscillator · Voltage conversion interface · Thermoelectric energy harvesting · Self-start-up · Thermoelectric generator · High conversion efficiency

1 Introduction

Thermoelectric generators (TEGs) used as energy harvesters have several advantages for autonomous systems such as low maintenance, long operating lifetime as well as vibration- and pollution-free operation [1, 2]. While conventional macroscale thermoelectric generators are only found in niche applications due to their limited power-efficiency [3], recent advances in micro- [4] and nanotechnology [5–7] combined with the use of low-dimensional materials [8] paved the way towards micro- and nanoscale TEGs with much higher power-efficiency and even opened-up new application ranges. For instance, the integration of TEGs in microelectronics enables harvesting of waste heat from hotspots [9, 10] for potential applications involving autonomous sensors [11], wireless systems [1] or for increasing battery life [6]. Microscale TEGs (microTEGs) have been fabricated for operation with in-plane [12] or cross-plane heat-flux configurations [13–16], and can be integrated on a wide range of substrates, including

Supplementary Information The online version of this article contains supplementary material available (https://doi.org/10.1007/s42452-022-05037-5).

✉ S. Tappertzhofen, stefan.tappertzhofen@tu-dortmund.de | [1]Chair for Micro- and Nanoelectronics, Department of Electrical Engineering and Information Technology, TU Dortmund University, Dortmund, Germany. [2]Institute for Integrated Circuits, Hamburg University of Technology, Hamburg, Germany. [3]Chair for Intelligent Microsystems, Department of Electrical Engineering and Information Technology, TU Dortmund University, Dortmund, Germany.

silicon [17] and flexible polymers [13, 18]. Due to their geometric constrains, microTEGs typically show relatively large internal resistances in a range of 10^1 – 10^3 Ω and can only provide small open-circuit voltages of typically V_{TEG} = 30 mV – 300 mV [13, 17, 19, 20]. The load-resistance of microelectronic devices is often not matching such large internal resistances and/or require higher supply-voltages. Therefore, voltage converters that are compatible with the limitations of microTEGs are required to provide sufficiently high supply-voltages to power microelectronics [21]. However, voltage converters reported in literature do either not provide high efficiency, for example < 60% [22–26], or often require external power supplies or signals for startup [24, 27–29]. These disadvantages make most voltage converters not compatible with the limitations of microTEGs and application in autonomous systems, which require full and independent self-startup functionality.

In this study we report on a two-stage voltage converter with full self-startup functionality from an open-circuit source voltage as low as 131 mV, which corresponds to a minimum converter input voltage of V_{in} = 65.5 mV. No additional external power supply is required at any time during operation.

The converter can be operated at high efficiency > 68% with a large range of source impedances ranging from 20.6 Ω to 4 kΩ, which is a much larger impedance range compared to concept reported so far. After self-startup, the converter achieves a maximum conversion efficiency of between 68 and 79% over the entire impedance range by using a novel dynamic maximum power point tracking concept.

The outline of the manuscript is as follows: at first, state-of-the-art voltage converters as well as the limitations of microTEGs are shortly introduced. Next, the proposed concept of a two-stage voltage converter with full self-startup functionality and dynamic maximum power point tracking is introduced. Section 4 summarizes the experimental details of the printed circuit board prototype and the simulation details. The experimental and simulation results are shown and discussed in Sect. 5 followed by a short conclusion.

2 State-of-the-art voltage converters for microTEGs

In the simplest case, the equivalent circuit of a microTEG is composed of a series connection of the actual thermoelectric open-circuit voltage source V_{TEG} and an internal resistance R_{TEG} (Fig. 1). The input voltage V_{in} of an external circuit with a load resistance connected to the microTEG, i.e. here a converter circuit, is given by V_{TEG} and the voltage drop V_R across R_{TEG}. When the load resistance is much larger than R_{TEG} it follows $V_{in} \approx V_{TEG}$. Typical ranges for R_{TEG} and V_{TEG} are 10^1 – 10^3 Ω and 30 mV – 300 mV, respectively [13, 17, 19, 20]. It should be noted that this equivalent circuit is appropriate for approximation of the steady-state operation of a microTEG on which we mainly focus in this study. To simulate the dynamic operation such as fluctuating internal resistance or generated voltage, a more complex equivalent circuit is required. Such an equivalent circuit may account for the microTEG's time constants determined by its thermal mass. In addition, external parameters such as convection or radiation may also affect the microTEG's Seebeck coefficients, and thermal and electrical impedances.

Advanced microTEGs provide maximum power-densities of some mW/cm^2 [14]. For comparison modern microelectronics have a heat power dissipation density of up to 1000 W/cm^2 [30]. Typical supply-voltages for embedded microelectronics or ultra-low-power microcontrollers range from 1.8 to 3.3 V [31]. Therefore, dedicated voltage converters that are compatible with the performance limitations of microTEGs are required to provide sufficiently high supply-voltages for microelectronics.

The following design criteria need to be fulfilled by a microTEG-compatible voltage converter [32]:

- Full and independent self-startup functionality, that is no requirement for external power supplies and control-signals for autonomous applications.
- Compatibility to low input voltages V_{TEG} = 30 mV 300 mV and relatively high generator internal resistances $R_{TEG} = 10^1$ 10^3 Ω.
- High conversion efficiency to prevent further decrease of the already small thermoelectric conversion efficiency.

Most voltage converters are based on either Meissner oscillators (Fig. 1a), boost converters (Fig. 1b), flyback converters (Fig. 1c), or a combination of these circuits. The operation principle of each converter is here only shortly introduced. Further details of the converter concepts can be found in Refs. [21, 33, 34].

In the Meissner oscillator, T_{M1}, C_{M2} and the coupled inductors N_P and N_S, which are typically realized by a transformer with opposite windings, form a self-triggered oscillator. C_{M1} is an input buffer-capacitor. Voltage conversion from an input voltage V_{in} to an output voltage $V_{M,out}$ is achieved by self-oscillated electromagnetic charging and discharging of the coupled inductors. $V_{M,out}$ drives an output current $I_{M,out}$ when an external load R_L is connected. Note, although N_P and N_S are part of the oscillator, they determine the transient increase of the output-voltage, and its amplitude is only slightly affected by the winding resistances. Thus, the magnitude of $V_{M,out}$ is almost

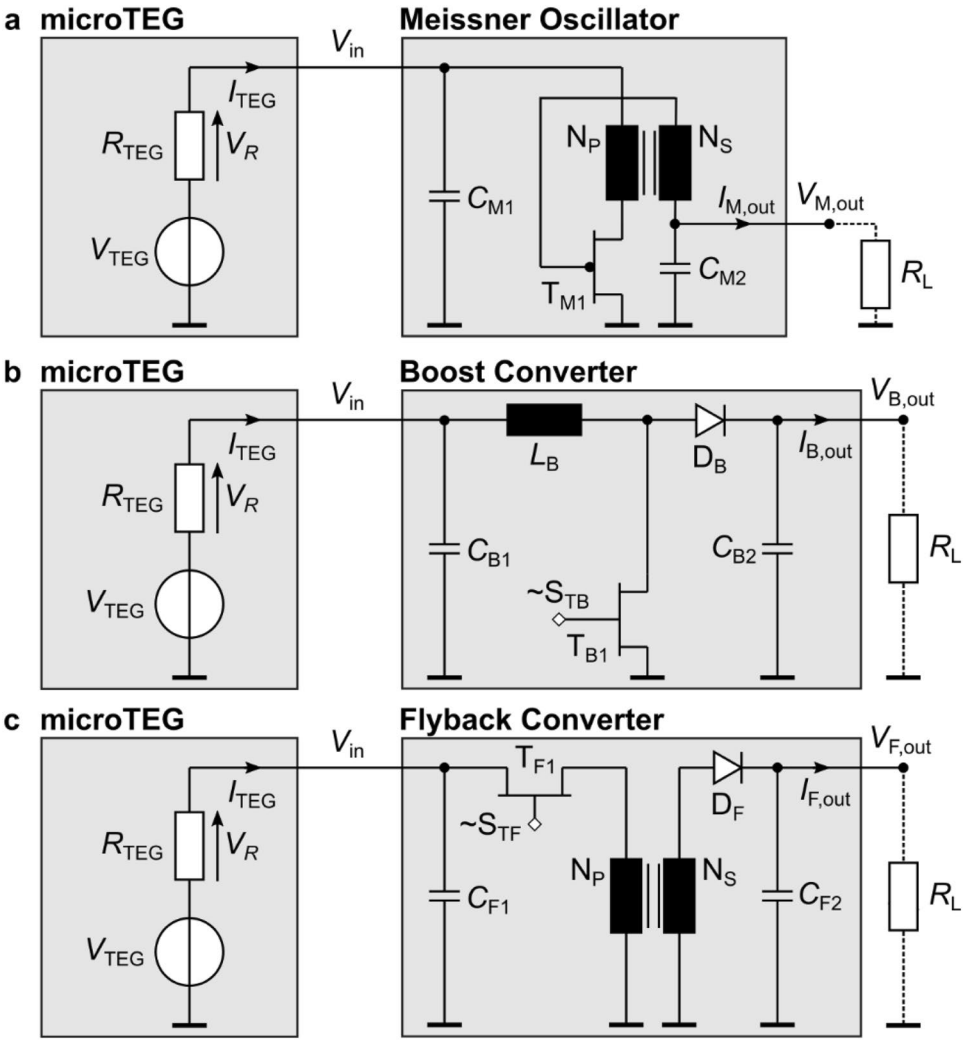

Fig. 1 Schematic circuits of state-of-the-art voltage converters with equivalent circuits of a thermoelectric generator. (a) Meissner oscillator, (b) boost converter, and (c) flyback converter

independent on the selected transformer. $V_{M,out}$ can be fixed to a maximum output voltage by e.g. using a Zener diode (not shown here).

In boost converts, which belong to the class of switched-mode power supplies [35], an external control signal ~ S_{TB} is required for charging and discharging of an inductor L_B. A rectifying diode D_B is used to allow the output current $I_{B,out}$ only to be driven in one direction. Here, the output voltage is $V_{B,out}$, and C_{B1} and C_{B2} are input and output buffer-capacitors, respectively.

In a flyback converter, charging and discharging is also achieved using a control signal ~ S_{TF}. Similar to a Meissner oscillator coupled inductors, which are usually realized by a transformer with opposite windings as well, are used. Compared to a boost converter, the flyback converter has typically slightly smaller efficiencies due to the non-ideal coupling of both inductors. In contrast to the Meissner oscillator, the output voltage $V_{F,out}$ depends on the ratio between the windings of N_P and N_S. A flyback converter allows in principle for galvanic insulation between V_{in} and $V_{F,out}$. C_{F1} and C_{F2} are input and output buffer-capacitors. D_F is required to allow the output current $I_{F,out}$ only to be driven in one direction.

The performance of voltage converters can be compared by the relative efficiency η, that is given by the converter's in- and output-power P_{in} and P_{out}, respectively:

$$\eta_r = \frac{P_{out}}{P_{in}} = \frac{V_{out} \bullet I_{out}}{V_{in} \bullet I_{TEG}} = \frac{{V_{out}}^2}{R_L \bullet V_{in} \bullet I_{TEG}} \quad (1)$$

Boost and flyback converters have high efficiencies typically above 70%. However, they require control signals for voltage conversion and therefore an external power supply for startup. In contrast, Meissner oscillators do not require any external power supply nor signals but have significantly lower efficiencies < 60% than boost and flyback converters [29, 36]. A straightforward method is to combine a Meissner oscillator with a boost converter for example to provide a voltage converter with self-startup functionality and high

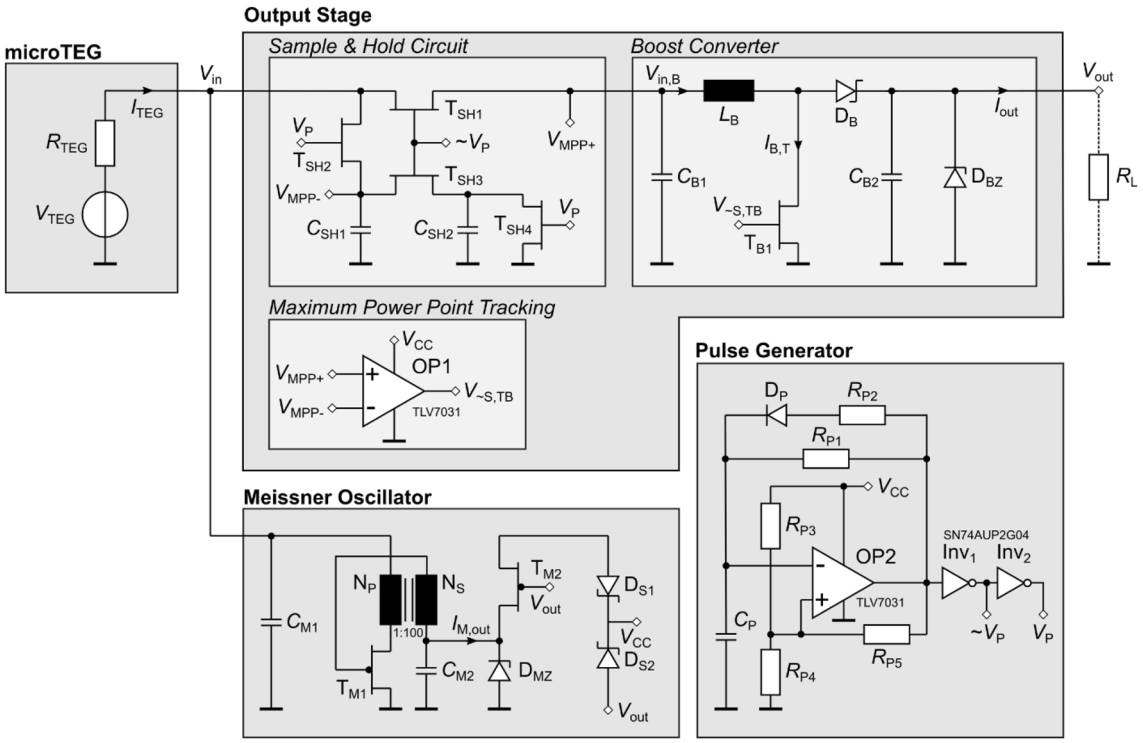

Fig. 2 Circuit implementation of the proposed self-startup voltage-converter circuit. The internal voltage V_{CC} is provided by the oscillator upon startup. Afterwards, V_{CC} is provided by the boost converter. The circuitry is operating at all time without any additional external power supply

conversion efficiency. Additional efficiency improvement is achieved using maximum power point tracking (MPPT). This allows to obtain a good impedance matching between the microTEG power source and the voltage converter [37, 38]. However, most concepts reported in literature are still suffering from poor efficiency [22–26], or require external signals or even power supplies for startup [24, 27–29]. Very recently, Dillersberger et al. reported on an integrated bipolar voltage converter with full self-startup functionality and high efficiency of 85% [39]. A Meissner oscillator is used for startup while a flyback converter is used for normal operation. However, the authors report on a limited source impedance range of $0 < R_{TEG} \leq 60\ \Omega$, which is much smaller compared to typical source impedances of up to $10^3\ \Omega$ of microTEGs. The study by Dillersberger et al. does not report whether the converter is compatible with the limitations of microTEGs. In addition, the output voltage depends on N_P:N_S, thus, one may not be flexible in using transformers with different footprints and windings

3 Concept of a high efficiency voltage converter for microTEGs

We propose a two-stage voltage converter with full and independent self-startup functionality. Although the converter has been designed for microTEGs, it is high flexibility. The concept is compatible to a large range of source impedances while simultaneously maintaining a high efficiency between 65 and 79%. This makes it possible to use the converter for bulk TEGs and many other energy harvesters as well. The complete circuitry is shown in Fig. 2. Upon startup, the Meissner oscillator (first stage) generates an internal voltage V_{CC} to supply the pulse generator. As soon as the pulse generator is in operation, a boost converter (second stage) with dynamic MPPT generates the output voltage with high conversion efficiency. In this case, T_{M2} is switched off and the pulse-generator is then also only supplied by the boost converter. The Meissner oscillator is then operating in open circuit condition. Thus, after startup the contribution of the Meissner oscillator's poor efficiency to the overall converter efficiency is small. Note, the whole circuitry, including the pulse-generator, operation amplifiers and inverters are only operated using a single input voltage V_{in}. No additional control, clock or reference signals are required.

3.1 Working principle of the dynamic maximum power point tracking

Since the performance of the microTEGs can change over time, e.g. by change of the heat flux, dynamic impedance matching is required to operate the converter with maximum efficiency. In the work by Dillersberger et al. this is achieved by setting up an appropriate switching frequency, which controls the converter's input resistance [40]. Hence, the frequency needs to re-programmed in case of performance variation of the microTEG for impedance matching. In the paper by Im et al. a similar MPPT circuitry like here is used, which, however, requires external control signals [32].

In the concept shown here flexible impedance matching is achieved using dynamic maximum power point tracking. The internal reference voltage for MPPT is V_{MPP+}. A conventional MPPT compares the converter's input voltage with a reference voltage that corresponds to the voltage for perfect impedance matching. Impedance matching is then provided by the MPPT setting up and appropriate switching frequency of T_{B1}. Here, instead of using a fixed reference-voltage for MPPT, a Sample & Hold (S&H) circuit continuously generates a variable reference voltage V_{MPP-}. The S&H circuit [28, 32] is controlled by an internal pulse generator. When V_P is high and consequently the inverted signal $\sim V_P$ is low, T_{SH1} is switched off and insulates the S&H from the boost converter. C_{SH2} is then discharged, and the voltage drop across C_{SH1} is equal to the open-circuit voltage of the microTEG. When V_P is low, the microTEG is connected to the boost converter. The voltage-drops across C_{SH1} and C_{SH2} are half of the microTEG's open circuit voltage V_{TEG}, thus $V_{MPP-} = V_{TEG}/2$. For MPPT operation, comparator OP1 compares V_{MPP+} and V_{MPP-}. If $V_{MPP+} > V_{MPP-} = V_{TEG}/2\,T_{B1}$ is switched on and charges L_B. This results in an increase of I_{TEG}, and thus, an increase of the voltage-drop across R_{TEG} until $V_{MPP+} \leq V_{MPP-}$. As soon as $V_{MPP+} \leq V_{MPP-}$, T_{B1} is switched off and the stored energy in L_B is supplied to the output-buffer capacitor. D_B prevents a current driving backwards. Consequently, I_{TEG} decreases and so does the voltage-drop across R_{TEG}, until $V_{MPP+} > V_{MPP-}$. In steady state, the internal input voltage of the boost converter will be $V_{MPP-} = V_{TEG}/2$, which corresponds to the case of perfect impedance matching:

$$P_{in} = V_{in} I_{TEG} \equiv P_R = V_R I_{TEG} = \left(V_{TEG} - V_{in}\right) I_{TEG}$$

$$\rightarrow V_{in} = \frac{V_{TEG}}{2}$$

4 Experimental and Simulation Details

We prepared a prototype PCB-board for experimental verification of the operation principle and self-startup functionality of the proposed voltage converter. The voltage signals were probed using a Tektronix TDS 1001B oscilloscope with a bandwidth 40 MHz. Quasi-static voltages were measured using an Escort 3136 A multimeter. V_{TEG} was provided by an external precision power supply (S160, Knick GmbH, Germany) and R_{TEG} was varied between 12 and 4 kΩ using a potentiometer in series to V_{TEG}. The MPPT, pulse generator and boost converter circuit were additionally simulated by LT Spice using a constant output of the Meissner oscillator of 3 V. Table 1 shows a list of the circuit components.

For operation of the Meissner oscillator, a *p*-JFET is required (the capacitive gate-input of a MOSFET would not lead to an oscillation). The transformer is based on a WE-EHPI (Würth Elektronik, Germany) with an inductivity of 7 µH on the primary side and 70 mH on the secondary side. The parasitic resistances on the primary and secondary side are 0.085 Ω and 205 Ω, respectively. Note, for simulation an ideal coupling-factor of 1 is assumed between the primary and secondary side. Schottky diodes D_B, D_{S1} and D_{S2} are used due to their low forward voltage drop. The pulse generator uses a fast switching-signal diode and is optimized for a frequency range of some hundreds of Hz and short pulse peaks (length

Table 1 Circuit components for the experimental prototype and LT Spice simulation

Part	Component/Value
C_{B1}	10 µF
C_{SH1}, C_{SH2}	27 nF
C_{M1}, C_{M2}, C_{B2}	1 µF
C_P	15 nF
D_B, D_{S1}, D_{S2}	Schottky diode (BAT41)
D_P	Switching-signal diode (1N4148)
D_{BZ}, D_{MZ}	Zener diode, 6.8 V (BZX55C6V8)
Inv_1, Inv_2	Inverting buffer (SN74AUP2G04)
OP1, OP2	Comperator (TLV7031)
L_B	10 mH, 2.6 Ω (1,410,606 C)
N_P:N_S	1:100, Würth WE-EHPI
T_{B1}, T_{SH1} – T_{SH4}	*n*-MOSFET (RHK005N03)
T_{M1}	*p*-JFET (J270)
T_{M2}	*p*-MOSFET (IRF9Z34NPbF)
R_{P1}	2.2 MΩ (5 MΩ potentiometer)
R_{P2}	600 kΩ (5 MΩ potentiometer)
R_{P4}	510 kΩ
R_{P5}	10 MΩ

Fig. 3 Picture of the printed circuit board of the self-startup voltage-converter circuit. The circuit board has contact pads and jumpers for analysis of voltage/current signals with electrical probes

some hundreds of µs). A TLV7031 for OP1 and OP2 is chosen, which has a quiescent supply current of 315 nA. An inverting buffer with 900 nA max. static current has been selected due to its low power consumption. The *n*- and *p*-MOSFET types were used due to their low on-state resistance, respectively. D_{BZ} limits V_{Out} to 6.8 V. Here, for $R_L \geq 100$ kΩ the output voltage is limited by the load resistance. A picture of the printed circuit board of the voltage-converter is shown in Fig. 3.

5 Results and discussion

5.1 Experimental proof-of-concept

Figure 4 depicts experimental results of the voltage converter prototype for $V_{TEG} = 300$ mV, $R_{TEG} = 98$ Ω. In Fig. 4a the output voltages V_P and $\sim V_P$ of the pulse generator are shown. The pulse generator frequency $f_P \approx 20$ Hz and pulse length (duty cycle) set by C_P, R_{P1} and R_{P2}. Here, the length is ≈385 µs, which equals a duty cycle of 0.019. The pulse generator controls the S&H circuit, which generates a dynamic reference voltage $V_{MPP\_} = V_{TEG}/2$. As can be seen, the dynamic maximum power point tracking automatically regulates the internal boost converter's input voltage to $V_{B,in} \approx V_{TEG}/2$. The peaks (A) correspond to events when V_P = high, in which C_{SH1} is charged to V_{TEG} and C_{SH2} is discharged. When V_P = low, the charge is equally distributed to C_{SH1} and C_{SH2} resulting in a voltage drop of $V_{TEG}/2$. The dynamic maximum power point tracking results in a ripple on $V_{B,in}$ of ± 13 mV as can be seen in the zoom in $V_{B,in}$ in Fig. 4c. The switching signals of the charging transistor T_{B1} determine the ripple frequency ≈ 3.85 kHz and are shown for comparison in Fig. 4c as well. The simulation reveals a power consumption of the pulse generator of 4.7 µW and of the MPPT of 7.2 µW. Thus, the total power consumption of the dynamic impedance matching is 11.9 µW. Figure 4d shows the results of the voltage conversion. As discussed above, the Meissner oscillator is used during startup to act as a power supply for the pulse-generator and the MPPT. The oscillation generates an internal output

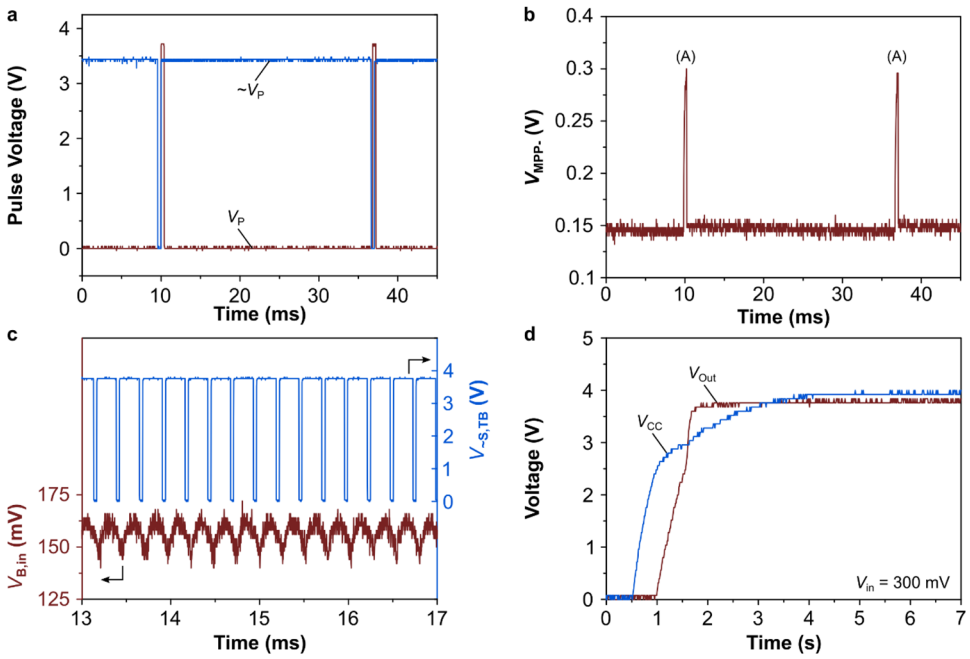

Fig. 4 Experimental results of the voltage converter. **a** Pulse generator output voltages V_P and $\sim V_P$. **b**) easurement of $V_{MPP\_}$ of MPPT. Peak (A) correspond to events in which the open-circuit voltage of the TEG is updated. **c** Zoom of the internal input voltage $V_{B,in}$ and measurement of the switching voltage $V_{\sim S,TB}$ for T_{B1} for comparison. **d** Measurement of the internal voltage V_{CC} and the output voltage V_{out}

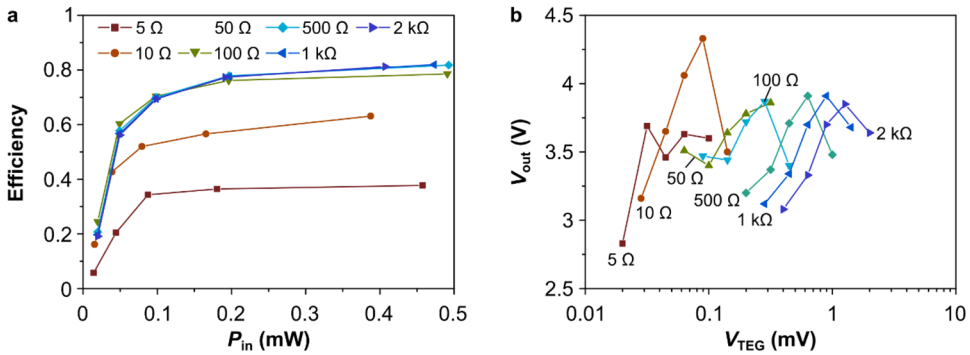

Fig. 5 LT Spice simulation results. **a** Converter efficiency vs. input power P_{in} for various R_{TEG}. **b** V_{out} vs. V_{TEG} for various R_{TEG}

voltage of the Meissner oscillator of $V_{CC} \approx 2.5$ V after 0.5 s. This is sufficiently high to supply the pulse generator and operate the boost converter and MPPT. Consequently, the Meissner oscillator is disconnected from V_{CC} via off-switching of T_{M2}. The complete circuit and an external load are now supplied by the boost converter. The maximum output voltage is regulated to 3.7 V. With $R_L = 100$ kΩ, this equals an output power of 137 µW and steady state current of 37 µA, which is sufficient to supply ultra-low power microcontrollers such as the ADuCM3027 (30 µA/MHz in active mode and 0.75 µA for hibernation).

The operation principle has been also experimentally verified by variation of R_{TEG} from 12 Ω to 4 kΩ and V_{TEG} between 30.7 and 1148 mV. Note, the performance demonstrated in most studies in literature [32, 41–44] are specified for a given input voltage V_{in} rather than for the open-circuit voltage V_{TEG}. Thus, due to the voltage-drop across R_{TEG} the open-circuit voltage for the microTEG needs to be higher than the input voltage specified in most studies. Here, the voltage converter can convert voltages from as low as $V_{TEG} = 30.7$ mV, i.e. $V_{in} = 15.35$ mV. However, a larger voltage is required for full self-startup. For 51 Ω we found a minimum self-startup voltage of $V_{TEG} = 202$ mV, i.e. $V_{in} = 100.5$ mV, and for 660 Ω we found $V_{TEG} = 726$ mV, i.e. $V_{in} = 363$ mV. The smallest self-startup voltage of $V_{TEG} = 131$ mV, i.e. $V_{in} = 65.5$ mV, was found for $R_{TEG} = 21.6$ Ω with an efficiency of 68%.

5.2 Performance and potential of further improvements

The overall goal in this study is to develop a voltage converter concept that fulfills the requirements for autonomous microTEG applications listed in Sect. 2. Table 2 shows a list of commercially available voltage converters (LTC 3108, LTC 3109, ECT 310, BQ25504) and research concepts. The experimental results of our prototype demonstrate full and independent self-startup functionality from V_{TEG} as low as 131 mV for $R_{TEG} = 21.6$ Ω, since apart from the microTEG no additional voltage supply or signal sources are required for operation. LT Spice simulations were done to analyze the performance of the proposed voltage converter for R_{TEG} between 5 Ω to 4 kΩ and V_{TEG} between 30.7 mV and 1790 mV. The same or at least similar components/models have been used for simulation and design of the experimental prototype.

Figure 5a depicts the converter efficiency (equ. (1)) by variation of the input power P_{in} and R_{TEG}. Note, P_{in} can be found without knowing I_{TEG}:

$$P_{in} = V_{in} \bullet I_{TEG} = V_{in} \bullet \frac{V_{TEG} - V_{in}}{R_{TEG}}$$

A simple model for a theoretical total loss balance is discussed in Supplementary Information S1. Theoretically, an efficiency of 85% is found in the ideal case, which is as expected larger than what is found in the simulations and experimentally. However, it is difficult to estimate a theoretical total loss balance or a limit of the efficiency of the proposed voltage converter since the performance and efficiency of the individual electriconic components is important. For example, the efficiency depends on the On resistance of the transistors, the transformer coupling factor, and the power consumption of the operation amplifier. Our simulation data already accounts for these parameters with the exception of the coupling factor of the transformer, for which we assume the ideal case of 1. Note, a smaller coupling factor is limiting the Meissner oscillator performance mainly during startup. In steady-state operation the output voltage is generated by the boost conveter and the loss contribution of the Meissner osciallator depends on the leakage current of T_{M1}, T_{M2} and D_{MZ}.

The experimental and simulation results reveal that the fundamental design criteria for voltage converters for autonomous microTEG applications are fulfilled. In particular, the voltage converter can be operated with relatively high microTEG impedances and a low input voltage. However, a minimum voltage of at least $V_{in} = 65.5$ mV is required for full self-startup. The overall efficiency of the converter is between 68% and 79%, which is competitive

Table 2 Literature Overview of voltage converter circuits

Ref.	Self-Startup	Min. V_{in} (mV) [a)]	R_{TEG} (Ω) [a)]	MPPT	Max. η [a)]
This work	V_{in} = 65.5 mV	15.35	21.6–4k	Yes	79.27%
Analog Devices, LTC 3108	V_{in} = 20 mV	20	1–10	No	60%
Analog Devices, LTC 3109	V_{in} = 30 mV	30	1–10	No	55%
EnOcean, ECT 310 Perpetuum	V_{in} = 20 mV	20	< 2	No	30%
Texas Instruments, BQ25504	V_{in} = 600 mV	130	n/a	Yes	> 90%
Shrivastava et al. [41]	V_{in} = 220 mV or RF-startup	10	2–10	Yes	83%
Carlson et al. [42]	V_{in} = 600 mV	20	3,9	No	75%
Gruber et al. [43]	V_{in} = 36 mV	36	≈ 1	No	68%
Kim et al. [27]	ext. battery	35	8	Yes	72% [b)]
Lhermet et al. [22]	n/a	1000	90	No	50%
Bautista et al. [28]	pre-charged capacitor, V_{in} = 900 mV	20	33,33–2,7k	Yes	61.15% [b)]
Ahmed et al. [28]	ext. battery, or V_{in} = 380 mV	12	n/a	No	82% [b)]
Ramadass et al. [23]	V_{in} = 35 mV + mechanical switch	25	5	Yes	58%
Im et al. [32]	V_{in} = 40 mV + ext, supply for control	40	5	Yes	61% [b)]
Doms et al. [24]	pre-charged capacitor, V_{in} = 2 V	640	100k	Yes	58%
Weng et al. [45]	V_{in} = 25 mV	15	6.2	No	73%
Dillersberger et al. [39]	V_{in} = ± 13 mV	± 13	0–60	Yes [b)]	85%

[a]Min. specified input voltage. The required input voltage depends on R_{TEG}. The max. efficiency may not be found at min. V_{in}. [b]The specified efficiency does not include the external supply for startup or converter control. [b)] The flyback converter includes a circuitry with similar functionality like MPPT for impedance matching. It should be noted that the concepts published by Kim et al., Im et al. and Dillersberger et al. use regulated output-voltages for improved voltage stabilization. However, this advantage decreases the total efficiency

to values for power-efficient voltage converters reported in literature, see Table 2. It should be noted that this efficiency is achieved for a large range of source impedances R_{TEG} = 20.6 Ω – 4 kΩ (for P_{in} > 180 µW and full self-startup functionality, see Fig. 5a), while for example an efficiency of up 85% of the converter reported by Dillersberger et al. is specified for only R_{TEG} = 0–60 Ω [39]. A similar large range of compatible source impedances has been reported by Bautista et al. [28]. However, their concept requires a much higher input voltage for self-startup 900 mV vs. 65.5 m V in this work, and shows a smaller efficiency of max. 61.15% vs. 68–79%.

Nevertheless, there is still potential for further improvement. For a proof-of-concept we designed a printed circuit board with discrete electronics as shown in Fig. 3. Obviously, this is not the ideal solution for a TEG application with microscale dimensions. However, all components can be in general integrated in an application specific circuit (ASIC) apart from the inductivity L_B, the transformer N_P:N_S as well as C_{B1} and C_{B2}. Usually in studies reporting on integrated voltage converters, these or similar components are externally connected to the voltage converter's integrated circuit. C_{M1}, and C_{M2} are also relatively large but are only used for the Meissner osciallator and may be optimized when the circuit, including the buffer inverters and comparators, are fully integrated on a single-low-power chip. A disadvantage of our converter is the external circuitry overhead by using a separate transformer and inductor L_B. This could be overcome by reusing the inductivity of the transformer's secondary side. Such a concept reduces the external circuitry and footprint, and has been reported by Dillersberger et al. for example [39]. However, for the flyback converter by Dillersberger et al. the ratio of N_P:N_S is critical for the output voltage amplitude. By adjusting the switching frequency of the boost converter, our concept has a higher flexibility in choosing an inductor L_B with small footprint. Therefore, the proposed voltage converter has a high potential for further improvement and area efficiency when the circuitry is modified for reusing the secondary side of the transformer.

6 Conclusions

In this study we demonstrated a concept of a voltage converter optimized for microTEGs with full and independent self-startup functionality from supply voltages as low as 65.5 mV, which corresponds to an open-circuit voltage of 131 mV. We demonstrated an experimental proof-of-concept and the performance potential was discussed based on LT Spice simulation. The converter is highly flexible and can be operated with a large range of source impedances ranging from 21.6 Ω to 4 kΩ while simultaneously maintaining a conversion efficiency between 68% up to a maximum efficiency of 79%. The proposed converter concept fulfills the requirements for voltage converters for fully

autonomous microTEG applications and can be used for many other energy harvesters due to its high flexibility.

Funding Open Access funding enabled and organized by Projekt DEAL. The authors have not disclosed any funding.

Data Availability The data that support the findings of this study are available on request from the corresponding author.

Conflict of interest The authors have no conflict to disclose.

References

1. Riffat S, Ma X (2003) Thermoelectrics: a review of present and potential applications. Appl Therm Eng 23:913–935
2. Wang X, Wang ZM (2014). In: Wang X, Wang ZM (eds) Nanoscale Thermoelectrics, vol 16. Springer, Cham
3. Boukai AI, Bunimovich Y, Tahir-Kheli J, Yu J-K, III Goddard WA, Heath JR (2008) Silicon nanowires as efficient thermoelectric materials. Nature 451: 168–171
4. Yan J, Liao X, Yan D, Chen Y (2018) Rev micro thermoelectric generator. J Microelectromechanical Syst 27:1–18
5. Hicks LD, Dresselhaus MS (1993) Effect of quantum-well structures on the thermoelectric figure of merit. Phys Rev B 47:12727–12731
6. Sullivan O, Gupta MP, Mukhopadhyay S, Kumar S (2015) On-chip power generation using ultrathin thermoelectric generators. J Electron Packag 137
7. Venkatasubramanian R, Siivola E, Colpitts T, O'Quinn B (2001) Thin-film thermoelectric devices with high room-temperature figures of merit. Nature 413:597–602
8. Hicks LD, Dresselhaus MS (1993) Thermoelectric figure of merit of a one-dimensional conductor. Phys Rev B 47:16631–16634
9. Aktakka EE, Ghafouri N, Smith CE, Peterson RL, Hussain MM, Najafi K (2013) Post-CMOS FinFET integration of bismuth telluride and antimony telluride thin-film-based thermoelectric devices on Sol substrate. IEEE Electron Dev Lett 34:1334–1336
10. Yang M-Z, Wu C-C, Dai C-L, Tsai W-J (2013) Energy harvesting thermoelectric generators manufactured using the complementary metal oxide semiconductor process sensors 13:2359–2367
11. Yang Y, Pradel KC, Jing Q, Wu JM, Zhang F, Zhou Y, Zhang Y, Wang ZL (2012) Thermoelectric nanogenerators based on single Sb-doped ZnO micro/nanobelts. ACS Nano 6:6984–6989
12. Zhang Q, Sun Y, Xu W, Zhu D (2014) Organic thermoelectric materials: emerging green energy materials converting heat to electricity directly and efficiently. Adv Mater 26:6829–6851
13. Zimmermann J, Merten D, Finke J, Drabiniok E, Fiedler H, Tappertzhofen S (2021) Scalable fabrication of cross-plane thin-film thermoelectric generators on organic substrates. Thin Solid Films 734:138850
14. Zhang W, Yang J, Xu D (2016) A high power density micro-thermoelectric generator fabricated by an integrated bottom-up approach. J Microelectromech Syst 25:744–749
15. Yu Y, Zhu W, Wang Y, Zhu P, Peng K, Deng Y (2020) Towards high integration and power density: Zigzag-type thin-film thermoelectric generator assisted by rapid pulse laser patterning technique. Appl Energy 275:115404
16. Liu S, Hu B, Liu D, Li F, Li J-F, Li B, Li L, Lin Y-H, Nan C-W (2018) Micro-thermoelectric generators based on through glass pillars with high output voltage enabled by large temperature difference. Appl Energy 225:600–610
17. Yuan Y, Najafi K (2019) Vertical self-defined thin-film thermoelectric thermocouples by angled co-evaporation for use in µTEGs. J Phys Conf Ser 1407:012014
18. Wang X, Suwardi A, Lim SL, Wei F, Xu J (2020) Transparent flexible thin-film p–n junction thermoelectric module. NPJ Flex Electron 4:19
19. Korotkov A, Loboda V, Dzyubanenko S, Bakulin E (2018) Fabrication and testing of mems technology based thermoelectric generator. In: 2018 7th Electronic System-Integration Technology Conference (ESTC) (IEEE), pp 1–4
20. Zhu XL, Li DS, Liu B, D, Zhe J (2012) Optimal design and simulation of a cross-plane micro-thermoelectric generator. Key Eng Mater 503:240–243
21. Twaha S, Zhu J, Yan Y, Li B (2016) A comprehensive review of thermoelectric technology: Materials, applications, modelling and performance improvement. Renew Sustain Energy Rev 65:698–726
22. Lhermet H, Condemine C, Plissonnier M, Salot R, Audebert P, Rosset M (2008) Efficient power management circuit: from thermal energy harvesting to above-IC microbattery energy storage. IEEE J Solid-State Circuits 43:246–255
23. Ramadass YK, Chandrakasan AP (2010) A batteryless thermoelectric energy-harvesting interface circuit with 35mV startup voltage. In: *2010 IEEE International Solid-State Circuits Conference - (ISSCC)* (IEEE) pp 486–7
24. Doms I, Merken P, Van Hoof C, Mertens RP (2009) Capacitive Power Management Circuit for Micropower Thermoelectric Generators With a 1.4µA Controller. IEEE J Solid-State Circuits 44:2824–2833
25. Woias P, Islam M, Heller S, Roth R 2013 A low-voltage boost converter using a forward converter with integrated Meissner oscillatorJ. Phys. Conf. Ser.**476**012081
26. Martinez T, Pillonnet G, Costa F (2018) A 15-mV Inductor-Less Start-up Converter Using a Piezoelectric Transformer for Energy Harvesting Applications. IEEE Trans Power Electron 33:2241–2253
27. Kim J, Kim C (2013) A DC–DC Boost Converter With Variation-Tolerant MPPT Technique and Efficient ZCS Circuit for Thermoelectric Energy Harvesting Applications. IEEE Trans Power Electron 28:3827–3833
28. Carreon-Bautista S, Eladawy A, Mohieldin AN, Sanchez-Sinencio E (2014) Boost Converter With Dynamic Input Impedance Matching for Energy Harvesting With Multi-Array Thermoelectric Generators. IEEE Trans Ind Electron 61:5345–5353
29. Desai NV, Ramadass Y, Chandrakasan AP (2014) A bipolar ± 40 mV self-starting boost converter with transformer reuse for thermoelectric energy harvesting *Proceedings of the 2014 international symposium on Low power electronics and design* vol 2015-Octob (New York, NY, USA: ACM) pp 221–6
30. Di Martino G, Tappertzhofen S (2019) Optically accessible memristive devices Nanophotonics 8:1579–1589

31. Uttarkar NK, Kanchi RR (2013) Design and development of a low-cost embedded system laboratory using TI MSP430F149 *2013 International Conference on Communication and Signal Processing* (IEEE) pp 165–75
32. Im J-P, Wang S-W, Ryu S-T, Cho G-H (2012) A 40 mV Transformer-Reuse Self-Startup Boost Converter With MPPT Control for Thermoelectric Energy Harvesting. IEEE J Solid-State Circuits 47:3055–3067
33. Damaschke JM (1997) Design of a low-input-voltage converter for thermoelectric generator. IEEE Trans Ind Appl 33:1203–1207
34. Zhou K, Yang S (2018) Smart Energy Management and ConversionComprehensive Energy Systemsvol5–5(Elsevier) pp 423–56
35. Villar-Piqué G, Alarcon E (2011) CMOS Integrated Switching Power Converters. Springer, Berlin, Heidelberg
36. Garcha P, El-Damak D, Desai N, Troncoso J, Mazotti E, Mullenix J, Tang S, Trombley D, Buss D, Lang J, Chandrakasan A 2017 A 25 mV-startup cold start system with on-chip magnetics for thermal energy harvesting *ESSCIRC 2017–43rd IEEE European Solid State Circuits Conference* (IEEE) pp 127–30
37. Yu C, Chau KT (2009) Thermoelectric automotive waste heat energy recovery using maximum power point tracking. Energy Convers Manag 50:1506–1512
38. Montecucco A, Knox AR (2015) Maximum Power Point Tracking Converter Based on the Open-Circuit Voltage Method for Thermoelectric Generators. IEEE Trans Power Electron 30:828–839
39. Dillersberger H, Deutschmann B, Tham D 2020 A Bipolar ± 13 mV Self-Starting and 85% Peak Efficiency DC/DC Converter for Thermoelectric Energy Harvesting *Energies* **13** 5501
40. Dillersberger H (2012) Flyback Converter for Operation with Very Low Input Voltages
41. Shrivastava A, Roberts NE, Khan OU, Wentzloff DD, Calhoun BH (2015) A 10 mV-Input Boost Converter With Inductor Peak Current Control and Zero Detection for Thermoelectric and Solar Energy Harvesting With 220 mV Cold-Start and – 14.5 dBm, 915 MHz RF Kick-Start. IEEE J Solid-State Circuits 50:1820–1832
42. Carlson EJ, Strunz K, Otis BP (2010) A 20 mV Input Boost Converter With Efficient Digital Control for Thermoelectric Energy Harvesting. IEEE J Solid-State Circuits 45:741–750
43. Gruber JM, Mathis S (2017) Kleine Temperaturdifferenzen optimal nutzen Elektronik 19:34–38
44. Ahmed KZ, Mukhopadhyay S (2014) A wide conversion ratio, extended input 3.5-μA boost regulator with 82% efficiency for low-voltage energy harvesting. IEEE Trans Power Electron 29:4776–4786
45. Weng P-S, Tang H-Y, Ku P-C, Lu L-H (2013) 50 mV-Input batteryless boost converter for thermal energy harvesting. IEEE J Solid State Circuits 48:1031–1041